Optically-induced charge separation and terahertz emission in unbiased dielectrics

W. M. Fisher[a] and S. C. Rand
Division of Applied Physics, Randall Laboratory, University of Michigan, Michigan 48109-1022, USA

(Received 14 December 2010; accepted 8 February 2011; published online 21 March 2011)

Charge separation mediated by linearly-polarized light in transparent insulators is analyzed numerically by integrating the equations of motion of a bound charge. It is shown that large static and transient dipole moments can be induced by the magnetic component of light at nonrelativistic intensities regardless of whether the pumplight is coherent or incoherent. Quantitative estimates show that efficient conversion of optical beams to electrical power is possible in lossless dielectric media and that THz radiation can be generated in unbiased materials through the use of transverse optical magnetism. © *2011 American Institute of Physics*. [doi:10.1063/1.3561505]

I. INTRODUCTION

Recent experiments have shown that intense magnetic dipole radiation can be generated with light at intensities as low as 10^7 W/cm^2 in transparent dielectrics.[1–3] This unexpected finding has been shown to take place via a magneto-electric interaction that was overlooked in the early days of nonlinear optics[4] and overcomes the apparent limitations on magnetic dipole (MD) effects imposed by the multipole expansion of classical electrodynamics.[5] It appears at sub-relativistic intensities due to parametric enhancement. Classical analysis,[2] numerical simulations and perturbation theory,[6] as well as quantum theory[7] of this phenomenon - transverse optical magnetism - have now been published. These treatments describe charge oscillations that are driven jointly by the electric and magnetic field components of a linearly-polarized light field. The fields act together (despite their orthogonality) to drive a dipolar magnetization parallel to the optical B field in bound electron systems. Strong coupling of energy from electric to magnetic motions accounts for the appearance of large magnetic dipole (MD) moments despite the weakness of optical Lorentz forces that exist at intensities far below the relativistic threshold ($I << 10^{18}$ W/cm^2).

In this paper we focus on the static charge displacement (and longitudinal electric field) that accompanies transverse optical magnetism. This phenomenon presents a striking contrast to the well-known but weak inverse Faraday effect which produces a small, quasistatic magnetic field along the direction of propagation of light when the polarization is circular.[8] It also contrasts with electric field generation by ponderomotive forces in plasmas, since transverse magnetism only experiences parametric enhancement in systems of bound charges.[9] The present effect induces a strong electric dipole moment along the propagation direction of linearly-polarized light by a mechanism involving both the optical electrical and magnetic field, making it quite distinct from optical rectification, a quadratic nonlinearity that arises only in noncentrosymmetric media and is purely electric.[10] We explain the origin of this magneto-electric effect and consider its implications for ultrashort pulse interactions and optical power conversion.

Numerical simulations of charge motion responding to the driving forces of incident light are presented in this paper to show that during magneto-electric interactions the centroid of electron motion shifts away from the nucleus. Each illuminated atom or molecule thereby acquires a large static dipole moment, while undergoing driven harmonic motion. This static polarization can be continuously sustained by steady illumination and arises from a complex sequence of events. First, the electric field initiates motion of electrons from rest, in a direction parallel to the electric field. Then the magnetic component of the light field causes a deflection of the electron around its axis. This small deflection due to the Lorentz force grows rapidly in amplitude as the result of a nonlinear parametric interaction[11,12] and the average position of the electron shifts away from the nucleus. The appearance of this static electric dipole along the axis of propagation is symptomatic of magnetic energy storage in the medium. Consequently, these steps result in the formation of an optically-charged capacitor that has the potential to provide an efficient source of electrical energy.

We also point out in this paper that when the incident field consists of a train of pulses, the quasistatic electric dipole described above develops a transient character that can lead to radiation at frequencies dictated by the pulse width with an amplitude dictated by charge transfer properties of the medium. Pulses of short duration are capable of generating radiation with a bandwidth as wide as $\Delta\nu \approx (1/\tau_p)$, where τ_p is the pulse width. For $\tau_p < 100$ fs, this bandwidth extends well into the THz range. Consequently, both optical charge separation and magnetically-induced terahertz (THz) radiation are predicted in this novel interaction. On the basis of these results, we evaluate a photo-voltaic generator concept that differs from conventional solar cells by not requiring absorption of the incident light or the generation of free electrons. We also propose THz generation in unbiased dielectrics.

II. Theory

To predict induced charge separation in bound electron systems, we consider a closed system of N identical, neutral

[a]Electronic mail: wfisher@umich.edu.

2-level atoms or molecules with a resonance frequency $\omega_0 = (\omega_2 - \omega_1)$. The atoms are subjected to an electromagnetic plane wave of frequency ω that propagates with a wavevector $\bar{k}$ in the positive z-direction. The light is assumed to be linearly-polarized along $\hat{x}$. Relevant results from earlier classical and quantum mechanical analyses of the induced magneto-electric response in such a system are summarized in the next two Sections.

A. Classical approach

The Lorentz oscillator model is a central paradigm of classical optics. It is based on a picture in which a single electron is bound to a nucleus by a harmonic potential and undergoes forced motion subject to damping. In this model, the driving forces are due to external electromagnetic fields which set the electron into motion according to the equation

$$\ddot{\bar{r}} + \gamma\dot{\bar{r}} + \omega_0^2\bar{r} = (q/m_e)[\bar{E} + \dot{\bar{r}} \times \bar{B}], \tag{1}$$

where $\bar{r}$ is the relative position vector from the nucleus to the electron, γ is a phenomenological damping coefficient, and q and m_e are the electron charge and mass, respectively. For the propagation direction and polarization specified above, the general equation of motion above reduces to two coupled differential equations:

$$\ddot{x} + \gamma_x\dot{x} + \omega_x^2 x = (qE_0/m_e)\cos(\omega t) - (qB_0/m_e)\dot{z}\cos(\omega t), \tag{2}$$

$$\ddot{z} + \gamma_z\dot{z} + \omega_z^2 z = (qB_0/m_e)\dot{x}\cos(\omega t). \tag{3}$$

Perturbative solutions of these equations, correct to first order in the weak optical magnetic field,[6] are

$$x(t) = \left(\frac{q}{m_e}\right)\frac{E_0}{\sqrt{(\omega_x^2 - \omega^2) + \gamma_x^2\omega^2}}\cos(\omega t + \varphi_0), \tag{4}$$

and

$$\begin{aligned} z(t) = &\frac{-\omega q^2 E_0 B_0}{2m_e^2\omega_z^2\sqrt{(\omega_x^2 - \omega^2)^2 + \gamma_x^2\omega^2}}\sin(\phi_0) \\ &+ \frac{1}{\sqrt{(\omega_z^2 - (2\omega)^2)^2 + \gamma_z^2(2\omega)^2}} \\ &\times \frac{\omega q^2 E_0 B_0}{2m_e^2\sqrt{(\omega_x^2 - \omega^2)^2 + \gamma_x^2\omega^2}}\sin(2\omega t + \phi_0 - \phi_1), \end{aligned} \tag{5}$$

where $\varphi_0 \equiv \tan^{-1}[-\gamma_x\omega/(\omega_x^2 - \omega^2)]$ and $\varphi_1 \equiv \tan^{-1}\{-2\gamma_z\omega/[\omega_z^2 - (2\omega)^2]\}$

The second term in Eq. (5) describes motion at twice the optical frequency, and gives rise to magneto-electric second harmonic generation,[13] but is not relevant to the present work. The first term of Eq. (5) for $z(t)$, which is the longitudinal charge displacement, is a zero frequency term corresponding to a static charge separation induced by the incident light in the neutral atom. This is optical rectification in a system with inversion symmetry, making it distinct from previously analyzed quadratic nonlinearities.[10] For continuous illumination, this result describes the formation of a sustained electric dipole moment and a corresponding electric field or voltage along the direction of propagation.

For illumination by ultrashort pulses, the implication is that THz radiation can be generated through impulsive rectification in unbiased, neutral dielectrics. This mechanism of THz generation is different from nonlinear electrical rectification in noncentro-symmetric media in two ways. First, the dipole generated by the ultrafast rectification lies along the direction of propagation rather than being perpendicular to it. Second, the indices of refraction for IR and THz radiation in a dielectric are much better matched than in most nonlinear crystals. For example, in fused silica the interaction described above will result in the generation of THz radiation in a Cerenkov cone with a half-angle of $\cos^{-1}(n_{IR}/n_{THz}) = 42$ degrees.[14] This angle is not as large as the Cerenkov cone angle in nonlinear crystals used for THz generation by conventional rectification, making it somewhat easier to extract the THz radiation from the nonlinear medium.

B. Quantum approach

The quantum mechanical analysis of this problem proceeds from the master equation for the density matrix

$$i\hbar\dot{\rho} = [H, \rho] - i\hbar\dot{\rho}_{relax}. \tag{6}$$

Since a full treatment has been given in the open literature,[7] only a brief summary is presented here. The system is assumed to consist of only two energy levels to make it as simple as possible. Its Hamiltonian $H = H_o + V(t)$ contains a time-independent part

$$H_o = \hbar\omega_1|1\rangle\langle 1| + \hbar\omega_2|2\rangle\langle 2|, \tag{7}$$

which describes the unperturbed diagonal matrix elements of the static Hamiltonian and an optical interaction $V(t)$ of the combined dipole form

$$V = -\bar{\mu}^{(e)} \cdot \bar{E} - \bar{\mu}^{(m)} \cdot \bar{B}. \tag{8}$$

$\dot{\rho}_{relax}$ represents phenomenological relaxation of individual density matrix elements in the Schrodinger picture. The pump light is assumed to be detuned by an amount $\Delta_1 \equiv \omega_0 - \omega$ from the electric dipole allowed transition at ω_0, as in the preceding Section.

Equation (6) can readily be solved for steady-state response by taking into account the electric field exactly and treating the magnetic field of the light as a perturbation. The result for the polarization of the system is found to be

$$\begin{aligned} \bar{P}(t) = N\hat{z}\Bigg(&\left\{\frac{1}{2}\frac{\mu_{21}^{(e)}[\Omega_0^{\prime(m)}]_{12}[\Omega_0^{(e)}]_{12}}{[\Delta_1 + i\Gamma_{12}^{(e)}][\omega_\phi + i\Gamma_{12}^{(m)}]} + c.c.\right\}\Bigg) \\ &+ \left(\left\{\frac{1}{2}\frac{\mu_{21}^{(e)}[\Omega_0^{(m)}]_{12}[\Omega_0^{(e)}]_{12}}{[\Delta_1 + i\Gamma_{12}^{(e)}][\Delta_2 + i\Gamma_{12}^{(m)}]}e^{2i\omega t} + c.c.\right\}\right) \end{aligned} \tag{9}$$

Factors in the numerators of Eq. (9) are Rabi frequencies defined by $\Omega_0^{(m)} = \mu^{(m)}B_0/\hbar$, $\Omega_0^{(e)} = \mu^{(e)}E_0/\hbar$, and $\Omega_0^{\prime(m)} = \mu^{(m)}B_0^*/\hbar$. The electric and magnetic dipole transition

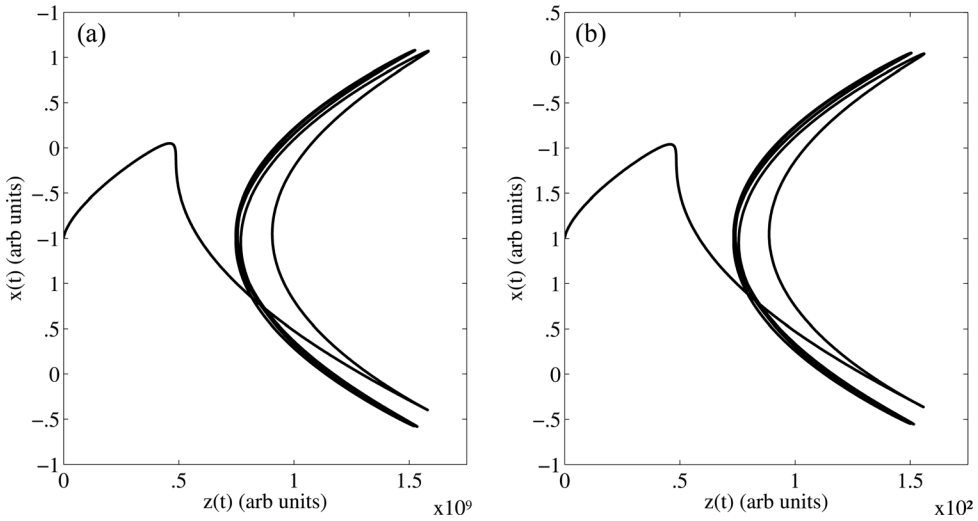

FIG. 1. (a) Trajectory of electron motion calculated by integration of the equations of motion for an incident electric field strength of $E_0 = 1$ V/m. Note the on the x and z axes differ by nine orders of magnitude. (b) Trajectory of electron motion for an incident electric field strength of $E_0 = 10^8$ V/m. Note the scales on the x and z axes are differ only by two orders of magnitude in this figure. Frequency and linewidth parameters were chosen to be $\omega = 1$, $\omega_x = \omega_y = 1.3$, $\omega_z = 1$ and $\gamma_x = \gamma_y = \gamma_z = 1$.

moments are $\mu^{(e)}$ and $\mu^{(e)}$ respectively. ω_φ is the resonant frequency for torsional (magnetic) oscillations about the axis of the B field.

Equation (9) contains two terms with different frequencies. The first is a zero frequency term that predicts a static charge separation induced by light in dielectric media illuminated by moderately intense light. This term is analogous to the first in the classical result of Eq. (5), except that the required microscopic symmetry is no longer exact inversion symmetry, as discussed in Ref. 7. It accounts for the charge separation and THz emission effects of interest in this paper, is proportional to the product E_0B_0 of field amplitudes, and is enhanced electronically when $\Delta_1 = 0$ or magnetically when ω_φ is small. However, it is independent of the parametric detuning factor Δ_2 because it is a static rather than a dynamic term. The second term is the radiant electric polarization mentioned in the last section that gives rise to longitudinally-polarized second harmonic radiation, but which is not of interest in this paper.

III. DISCUSSION

A. Charge separation in coherent fields

To follow the actual trajectory of an electron driven by the light field in real space, the time-dependent equations of motion must be solved. For this purpose, classical theory is perfectly adequate and Eqs. (4) and (5) can simply be integrated numerically, provided that the incident light field does not induce population changes. This latter requirement calls for the simulation of off-resonant excitation. In the simulations that follow (Figs. 2–5), the driving field is therefore detuned by more than one transition linewidth and field strengths are adjusted to correspond to either of two regimes: a low intensity regime where magnetic interactions are negligible and a high intensity regime where magnetically-driven polarizations attain their maximum amplitude with respect to the linear electric polarization of the medium.

Figure 1 presents two trajectories calculated by direct integration of the classical harmonic oscillator model *including* the magnetic Lorentz force see Refs. 2 and 6). In each plot, the optical field is applied as a step function at time zero and frequency is detuned from electronic resonance by $\Delta_1/\gamma_x = \Delta_1/\Gamma_{12}^{(e)} = 1.67$. Normalized frequency parameters were assigned fixed values of $\omega = 1$, $\omega_x = \omega_y = 1.5$, $\omega_z = 0.2$, $\gamma_x = \gamma_y = \gamma_z = 0.3$. Figure 1(a) is calculated for an incident plane wave field of $E_0 = 1$ V/m and Fig. 1(b) is for $E_0 = 10^8$ V/m. In the first case, at low field strength, the trajectory lies almost entirely along the x-axis of the electric field, as expected for low intensity optical interactions. Motion driven by the electric field dominates the dynamics overwhelmingly. Magnification of the horizontal scale by 10^9 is necessary to make the component of the motion in the direction of propagation of light large enough to see. It is this component that originates from the Lorentz force. In

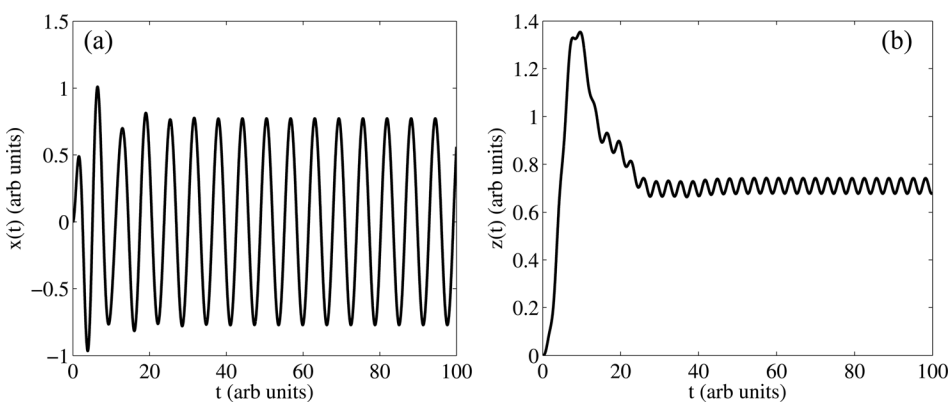

FIG. 2. Cartesian components of electron motion along (a) the x axis, and along (b) the z axis, calculated for $E_0 = 10^8$ V/m and $\tau_{coh} = \infty$. Frequency and linewidth parameters were chosen to be $\omega = 1$, $\omega_0 \equiv \omega_x = \omega_y = 1.5$, $\omega_\varphi \equiv \omega_z = 0.2$ and $\gamma_x = \gamma_y = \gamma_z = 0.3$.

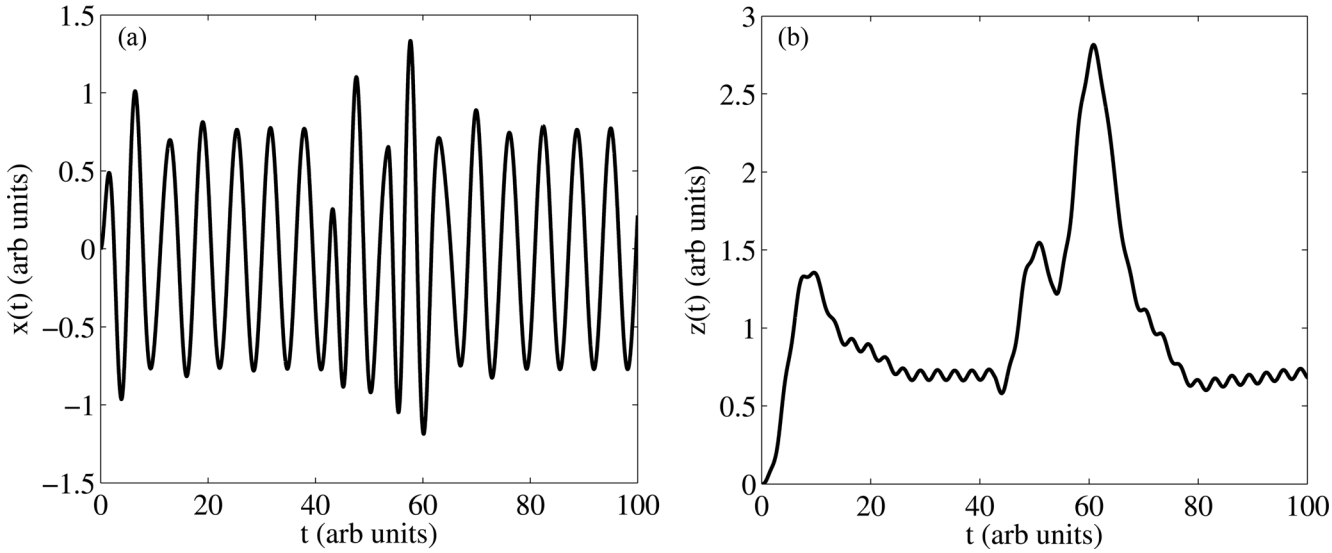

FIG. 3. Cartesian components of electron motion along (a) the x axis, and along (b) the z axis, calculated for $E_0 = 10^8$ V/m and an average phase disruption time of $\tau_{coh} = 30$ fs. Frequency and linewidth parameters are the same as in Fig. 2.

Fig. 1(b) on the other hand, the horizontal scale is only one hundredth that of the vertical axis. At slightly higher intensity, the motion along z develops an amplitude comparable to that of motion along x.

It can be seen from both of these figures that motion reaches a steady state after only a few periods. The deviations from linear response along the electric field direction appear on an ultrafast time scale in this simulation. The electron follows a strongly curved path and the centroid of the motion is displaced forward along the direction of propagation, away from the nucleus located at $x = y = z = 0$. Although E and B are similar in that they oscillate harmonically at the optical frequency and therefore have an average value of zero, E is a polar vector that reverses sign upon inversion, whereas B is an axial vector which does not. In combination, it is evident from Fig. 1 that these field components can drive a static displacement of bound electrons with respect to the nucleus. Remarkably, the exchange of energy that takes place between the electric and magnetic degrees of freedom in the system does not reverse as time progresses, as it does in other coupled oscillator systems. Here, the overall optical interaction at intermediate (sub-relativistic) intensities yields an electric dipole (ED) moment on an ultrafast time scale which is quasistatic and intensity-dependent. The large amplitude of this effect may be ascribed to the doubled frequency of electron motion projected along z [Figs. 2(b)–4(b) and 5(c)], and the orthogonality of the electric and magnetic driving fields, which introduces intense parametric enhancement of the magnetic response. Since the dynamics have been shown to obey a complex Mathieu equation (see Ref. 6), this result is not too surprising.

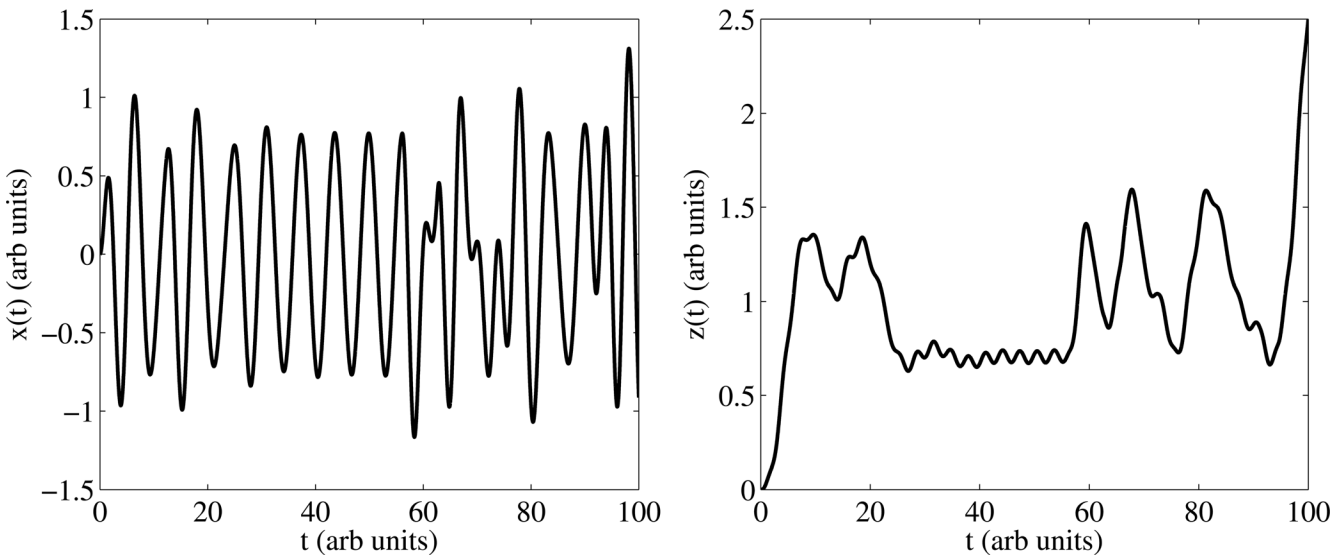

FIG. 4. Cartesian components of electron motion along (a) the x axis, and along (b) the z axis, calculated for $E_0 = 10^8$ V/m and an average phase disruption time of $\tau_{coh} = 3$ fs. Frequency and linewidth parameters are the same as in Fig. 2.

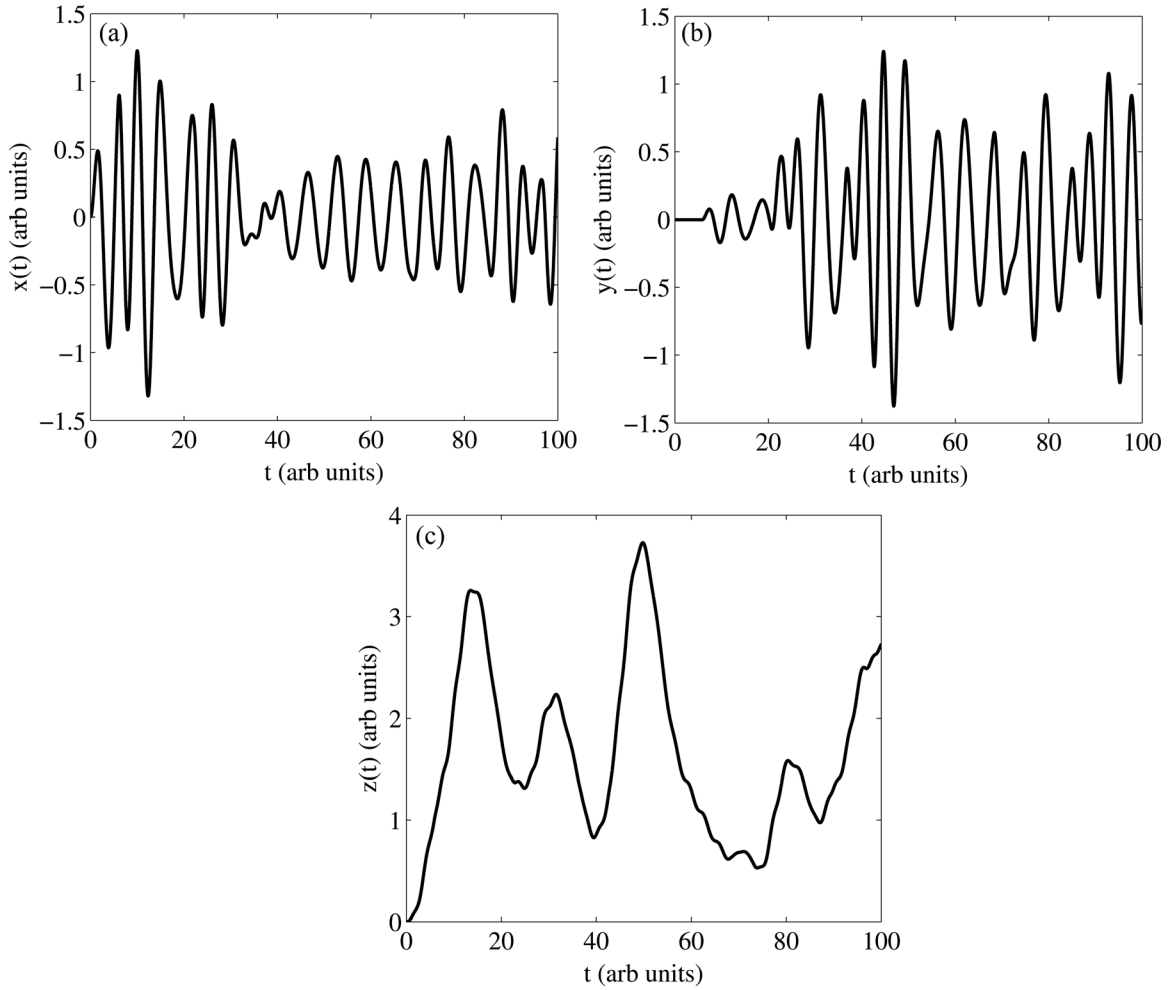

FIG. 5. Cartesian components of electron motion along (a) the x, (b) the y, and (c) the z axes, calculated for $E_0 = 10^8$ V/m and an average phase *and* polarization disruption time of $\tau_{coh} = 3$ fs. Frequency and linewidth parameters are the same as in Fig. 2.

B. Charge separation in stochastic fields

The Cartesian trajectories plotted in Fig. 1 were obtained by assuming a completely coherent driving field ($\tau_{coh} = \infty$). In this case, the system undergoes a forced oscillation that continues without variation after the first few periods. The Cartesian components of this charge motion are therefore seen to vary harmonically at long times in Fig. 2. The excursions along x and z are plotted separately in Figs. 2(a) and 2(b) for clarity, and reveal that the projection of circular motion on z doubles its frequency, in agreement with analysis in Ref. 2. These calculations provide a point of comparison with the driven response to stochastic fields. The effects of dephasing and depolarization are explored next in Figs. 3–5.

To follow charge motion driven by a random light field, an Euler integration technique[15] that employed a constant temporal step size was used. The stochastic character of sunlight was simulated by changing the phase of the driving fields by an amount in the range 0–2π at an average rate of τ_{coh}^{-1}. One hundred integration steps were performed per optical cycle. This permitted precise variation and specification of the coherence time. For example, at a wavelength of 800 nm the optical period is 2.6 fs, so a coherence time of 30 fs can be modeled accurately by randomly changing phase at an average rate of once per 1150 steps. The effect of a stochastic driving field with $\tau_{coh} = 30$ fs is presented in Fig. 3. When the dephasing time was reduced to 3 fs to correspond specifically to radiation from the sun, the results in Fig. 4 were obtained. Note that in both Figs. 4(a) and 4(b) a large, positive offset of the average motion is still evident in the direction of propagation, despite dephasing at rates approaching the optical frequency. It should be noted that the arbitrary unit scales of Figs. 3–5 are the same for easy comparison.

Sunlight exhibits rapid, random fluctuations both in phase and polarization. To simulate radiation from this source fully, the procedure described above must therefore be generalized to include stochastic polarization fluctuations. Allowance for random polarizations in the x-y plane necessitates an extension of the calculations above to three dimensions. Consequently in Fig. 5 the projection of the electron trajectory along y is presented in addition to the components along x and z. Polarization jumps were assumed to take place at the same time as phase jumps, but were based on a separate random number generator. Figures 5(a) and 5(b) jointly furnish a map of the electron motion in the transverse plane. By comparing similar plots where z is nearly constant, one

notices that decreases in the amplitude of motion along x invariably accompany increases in the amplitude along y and vice versa. In Fig. 5(c), the average displacement of the charge along z remains similar to that when phase-only disruptions are taken into account. Large random excursions and oscillations are evident in Fig. 5(c) but the average offset remains similar to that in Fig. 2(b). The average offset represents the DC voltage available for extraction but we emphasize that phase and polarization transients tend to increase rather than decrease the offset.

C. Optical-to-electrical power conversion

The charge separation described above saturates when the magnetic current density J_M attains its maximum value, namely one half the electric displacement current J_E.[2,7] At higher levels of excitation than this, in the so-called saturation regime, the magnetic susceptibility is

$$\chi^{(m)} = -\frac{1}{2}\chi^{(e)}, \tag{10}$$

and the longitudinal polarization established by it is proportional to the electric field, just like the usual transverse polarization induced by the electric field component of light. As we show next, through the use of Eq. (10), predictions can be made of the surface charge density attainable in a plane-parallel dielectric slab illuminated uniformly with a specified intensity of coherent light - without knowledge of the linewidth parameters, detunings and transition moments in Eq. (10). With this information, the electric energy density that can be stored in a magnetic "optical capacitor" may be accurately estimated in the undepleted pump limit.

The simplest way to calculate the energy U stored in a magnetic optical capacitor is to imagine a simple parallel plate capacitor formed by a dielectric slab of thickness L and permittivity ε through which the light propagates. Then, as is well-known,

$$U = \frac{1}{2}CV^2, \tag{11}$$

where C is the capacitance and V is the voltage that develops across the slab due to irradiation. The displacement charge Q that develops is given by the beam area A times the induced surface charge density σ_s.

$$Q = \sigma_s A \tag{12}$$

The magnitude of any surface charge density is the same as the polarization P per unit volume that causes it.[16] Hence, making use of Eq. (10) and the standard formula for the capacitance of a dielectric slab, we have

$$V = \frac{Q}{C} = \frac{\sigma_s A}{\varepsilon A/L} = \frac{P^{(m)}L}{\varepsilon} = \frac{-\frac{1}{2}\chi^{(e)}EL}{\varepsilon/\varepsilon_0} = -\frac{(\varepsilon_r - 1)EL}{2\varepsilon_r}, \tag{13}$$

where we note that in this case the polarization $P^{(m)} = -(1/2)\varepsilon_0\chi^{(e)}E$ is of magneto-electric origin, is diamagnetic, and equals half the usual electric polarization. In Eq. (13), use has also been made of the relationship $\chi^{(e)} = \varepsilon_r - 1$ between the susceptibility $\chi^{(e)}$ and the relative permittivity $\varepsilon_r = \varepsilon/\varepsilon_0$. Substitution of Eqs. (12) and (13) into (13) results in a stored energy of

$$U = \frac{1}{2}\frac{\varepsilon_0\varepsilon_r A}{L}\left[\frac{(\varepsilon_r - 1)EL}{2\varepsilon_r}\right]^2. \tag{14}$$

In the focal region of a fundamental Gaussian beam of radius ω_0, the relevant area and confocal parameter are given by[17]

$$A = \pi\omega_0^2 \tag{15}$$

and

$$L_{conf} = \frac{2\pi\sqrt{\varepsilon_r}\omega_0^2}{\lambda}. \tag{16}$$

Hence, if we ignore depletion of the optical pump wave, the expression for energy stored in the medium as the result of interacting with a Gaussian beam over the length L_{conf}, is

$$U_{\max} = \frac{\varepsilon_0\pi^2\omega_0^4}{4\lambda\sqrt{\varepsilon_r}}(\varepsilon_r - 1)^2E^2. \tag{17}$$

When the pump wave consists of laser light, the wavelength in Eq. (17) is that of the laser and ε_r is the permittivity at the laser wavelength. For solar input, representative values near the peak of the solar spectrum may be assumed. In the latter case it is important to note that the power conversion is operative at all wavelengths in the solar spectrum that fall within the transparency range of the conversion material. Hence, ε_r is determined by the off-resonance susceptibility and the entire spectrum is useful for power conversion.

For efficient optical power generation, the energy storage process that develops charge separation must be repeated as rapidly and as often as possible. In the case of sunlight, the direction of propagation of light in the slab should therefore alternate at a high rate Ω. Because the rise time of charge separation is faster than 100 fs (see Figs. 2 and 3 and Refs. 1 and 2), it is virtually instantaneous compared with attainable values of Ω^{-1}. Hence power extraction via conducting electrodes applied to the surface of the slab will be limited chiefly by Ω, assuming that the focused intensity achieves magnetic saturation. Assuming that all the stored energy is extracted during each cycle of beam reversal, the maximum generated power is expressible as

$$P_{\max} = \frac{\varepsilon_0\pi^2\omega_0^4}{2\lambda\sqrt{\varepsilon_r}}(\varepsilon_r - 1)^2\eta_0\Omega I, \tag{18}$$

where η_0 is the electromagnetic impedance of vacuum and I is the focused optical intensity

D. Power conversion efficiency

Estimates of the power levels and efficiencies of a converter based on magnetic charge separation can be made using Eq. (18). This equation incorporates the relationship between the length L_{conf} of the region over which focusing of a Gaussian beam can be maintained and the corresponding focal spot size ω_0. Hence, it will be applied first to estimate optical-to-electric power conversion of a single mode laser

beam, under the assumption that the focused intensity is adequate to saturate the chosen magnetic conversion medium. Then, a simple extension involving guided waves will be applied to remove the constraint between sample length L and spot size. This greatly improves efficiency and makes solar power conversion possible.

To estimate the optical-to-electric power conversion possible with a 1 kW fundamental Gaussian beam switched at a rate of $\Omega = 25$ MHz, we consider focusing it to a spot size of $\omega_0 = 50$ μm in a sample of sapphire of length $L_{conf} = 4.45$ cm. Taking the relative permittivity and wavelength to be $\varepsilon_r = 3.115$ and $\lambda = 800$ nm respectively, an extracted power of $P_{\max} = 1.04$ W is obtained. That is, the conversion efficiency is found to be just $\eta = P_{extr}/P_{in} = 0.114\%$. This estimate and the ones that follow ignore losses from coupling to external circuits with real loads, or to energy storage devices like batteries. This is because electrical coupling losses can be made quite small for capacitive energy sources using energy harvesting circuitry.[18]

Note that if the light were focused into an optical fiber of length L, it would be confined over lengths much longer than L_{conf}, regardless of spot size. Hence, we next consider a sapphire fiber of length $L = 10$ m, removing the constraint between sample length L and ω_0 given by Eq. (16). Single-crystal sapphire fibers have a favorably high index, high thermal conductivity, and can be grown in meter lengths by the laser-heated pedestal growth method.[19] In this situation, the expression for extracted power becomes

$$P_{\max} = \frac{\varepsilon_0 \pi \omega_0^2 L}{4\varepsilon_r}(\varepsilon_r - 1)^2 \eta_0 \Omega I. \tag{19}$$

For the same input power of 1.0 kW and a fiber core radius of ω_0=50 μm, the extracted power is now 0.299 kW at $\Omega = 25$ MHz. Under these conditions, ignoring pump depletion, the theoretical conversion efficiency climbs to $\eta = 30\%$.

On a sunny day at low latitudes, a spherical solar concentrator of diameter 1.0 m collects power roughly equal to that considered above, namely 1 kW. The concentrator may be assumed to be an f1 optic whose focal length equals its diameter. In practice this will focus sunlight as tightly as is practical. The sun subtends a relatively large angle $\alpha = 4.67$ mrad at earth, so sunbeams are not Gaussian beams. Instead, the focal image size ω_0 is a fixed fraction of the radius R of the concentrator: $\omega_0 = 4.67 \times 10^{-3} R$. For collected powers in the kW range, the focal spot size is therefore much larger than in the earlier estimates for a Gaussian beam source. The available focal spot intensity is limited to approximately $I_{avail} \sim 1.46 \times 10^7$ W/m^2, which is considerably lower than the intensity required for saturation of the optical magnetization in materials like CCl_4 that have values of I_{sat} exceeding 10^7 W/cm^2 (Ref. 3). Recognizing that the magnetic saturation intensity varies dramatically from one material to another,[3] and that available intensities may be lower than I_{sat}, a formula for the electrical power that can be extracted from a material with given I_{sat} at available light intensities is needed. With these constraints, the magnetic susceptibility is $\chi^{(m)} = -(I_{avail}/I_{sat})^{1/2}(\chi^{(e)}/2)$. Hence, the expression for power output becomes

$$P_{out} = \frac{\varepsilon_0 \pi (\varepsilon_r - 1)^2}{4\varepsilon_r} \omega_0^2 L \eta_0 \Omega \left(\frac{I_{avail}^2}{I_{sat}} \right). \tag{20}$$

The earlier discussion of Figs. 3–5 showed that the charge separation effect of interest here is not significantly reduced by dephasing or depolarization at rates approaching the optical frequency itself. Unlike interactions between linear oscillators, the transfer of energy between the electric and magnetic degrees of freedom of light resists disruption and is irreversible. Hence coherent light is not needed to drive the magneto-electric power generation described here. Taking this into account and using the expression for P_{out} in Eq. (20), the output of a solar converter based on magneto-electric conversion can be accurately predicted. As an example, we consider implementing a generator with a $\varphi = 1$ m diameter concentrator, a 1-cm diameter bundle of sapphire fibers each of which has a length $L = 10$ m and external circuitry consisting of several 50/1 step-down transformers and semiconductor rectifiers with reverse breakdown voltage ratings exceeding $V_B \geq 600$ V, for power conditioning. According to Eq. (13), and assuming $I_{avail}/I_{sat} = 0.1$ in a fiber core with the permittivity of sapphire, the end-to-end voltage generated in each fiber of the bundle is $V = 3.56 \times 10^5$ Volts. Using a representative wavelength of 0.6 μm for sunlight, and a beam switching rate of $\Omega = 25$ MHz as before, the extractable power is 29.7 W, yielding a theoretical efficiency of nearly 3%.

This scheme for optical power conversion is basically capacitive in nature. Hence, the voltages that develop across the conversion medium approach the megavolt range when the efficiency is pushed to high values, for example by extending fiber length. Although power extraction at high voltages can be handled using transformers and robust electronics,[18] the identification of materials with lowered intensity requirements will facilitate power generation by lowering the voltage levels that must be handled. Also, non-capacitive schemes may offer alternatives. By using pulsed or chopped input light, alternative implementations of this power generation scheme can be imagined that would exploit the transient, optical magnetization of the medium to produce current flow inductively. By passing the light through an array of conducting split rings whose diameters lie parallel to the propagation axis, single cycle voltage waves would be generated by each pulse passing through the medium, according to Lenz's Law. Designs based on this approach will be considered in a forthcoming publication.

IV. CONCLUSION

In summary, we have analyzed a new quadratic optical interaction that can mediate quasistatic charge separation and THz emission in transparent dielectric materials. A magneto-electric power generation scheme has been proposed that relies on displacement currents in insulators, and avoids both the absorption and the electron-hole pair production that typify semiconducting solar cells. Dephasing and depolarization of the pump light result in negligible reductions in the expected charge separation and magnetic energy storage. Hence for sufficiently high input power from a laser beam or

a solar concentrator, particularly in conjunction with the use of a waveguide and optimized conversion media, optical-to-electrical power conversion efficiencies of ~10% or more should be readily attainable.

ACKNOWLEDGMENTS

W.M.F. wishes to acknowledge support from an Applied Physics Fellowship of the University of Michigan. The authors wish to thank H. Hoffman and J. Nees for valuable discussions.

[1]S. L. Oliveira and S.C. Rand, Phys. Rev. Lett. **98**, 093901 (2007).
[2]S. C. Rand, W. M. Fisher, and S. L. Oliveira, J. Opt. Soc. Am. B **25**, 1106 (2008).
[3]W. M. Fisher and S. C. Rand, J. Lumin. **129**, 1407 (2009).
[4]Y. R. Shen, *The Principles of Nonlinear Optics* (J. Wiley & Sons, New York, 1984)
[5]L. D. Landau, E. M. Lifshitz, and L. P. Pitaevskii, *Electrodynamics of Continuous Media*, 2nd ed. (Pergamon Press, Oxford, 1984), p. 268.
[6]W. M. Fisher and S. C. Rand, Phys. Rev. A **82**, 013802 (2010).
[7]S. C. Rand, J. Opt. Soc. Am. B **26**, B120 (2009).
[8]J. P. van der Ziel, P. S. Pershan, and L. D. Malmstrom, Phys. Rev. Lett. **15**, 190 (1965).
[9]D. Dietze, J. Darmo, S. Roither, A. Pugzlys, J. N. Heyman, and K. Unterrainer, J. Opt. Soc. Am. B **26**, 2016 (2009).
[10]R. W. Boyd, *Nonlinear Optics* (Academic, New York, 1992), p. 42.
[11]M. Cartmell, *Introduction to Linear, Parametric, and Nonlinear Vibrations* (Chapman & Hall, New York, 1990).
[12]B. Y. Zeldovich, Physics-Uspekhi **51**(**5**), 465 (2008).
[13]M. Fiebig, D. Frohlich, Th. Lottermoser, V. V. Pavlov, R. V. Pisarev, and H.-J. Weber, Phys. Rev. Lett. **87**, 0137202 (2001).
[14]D. Kleinman and D. Auston, IEEE J. Quant. Elec. **20**, 964 (1984).
[15]R. W. Hamming, *Numerical Methods for Scientists and Engineers*, 2nd ed. (Dover, New York, 1986).
[16]A. Kip, *Fundamentals of Electricity and Magnetism*, 2nd ed. (McGraw-Hill, Toronto, 1969), pp. 129–135.
[17]A. Yariv, *Quantum Electronics* 3rd ed. (J. Wiley & Sons, New York, 1989), pp. 122–123.
[18]G. K. Ottman, H. F. Hofmann, A. C. Bhatt, and G. A. Lesieutre, IEEE Trans. Power Electron. **17**, 669 (2002).
[19]R. Nubling and J. A. Harrington, Appl. Opt. **36**, 5934 (1997).